

Energy Dependence of Light Nuclei (d , t) Production at STAR

Dingwei ZHANG¹ (for the STAR Collaboration)

¹Key Laboratory of Quark & Lepton Physics (MOE) and Institute of Particle Physics, Central China Normal University, Wuhan, 4300 79, China

E-mail: zhangdingwei@mails.ccnuc.edu.cn

(Received mm dd, 2019)

In high-energy nuclear collisions, the production of light nuclei is sensitive to the temperature and phase-space density of the system at freeze-out. In addition, the phase transition from QGP to the hadronic phase will lead to large baryon density fluctuation, which will be reflected in the light nuclei production. For example, the ratio of proton ($N(p)$) and triton ($N(t)$) to deuteron ($N(d)$) yields, which is defined as $N(t) \cdot N(p) / N^2(d)$, may be used as a sensitive observable to search for the QCD critical point. In this paper, we will report the energy dependence of light nuclei (d , t) production in Au+Au collisions at $\sqrt{s_{NN}} = 7.7, 11.5, 14.5, 19.6, 27, 39, 62.4, \text{ and } 200 \text{ GeV}$ measured by the STAR experiment at RHIC. We will present the beam energy dependence for the coalescence parameter $B_2(d)$ and $B_3(t)$, particle ratios (d/p , t/p , and t/d), and the yield ratio of $N(t) \cdot N(p) / N^2(d)$. Their physics implications will be discussed.

KEYWORDS: Triton, Coalescence parameters, Neutron density fluctuation

1. Introduction

In relativistic heavy-ion collisions, the most important goal is to study the properties of nuclear matter at high baryon density or temperature. The phase transition between the Quark-Gluon Plasma (QGP) and the hadronic matter is currently a topic of great interest [1]. Light nuclei are sensitive small binding energy, they are sensitive to the local nucleon density. Light nuclei production is described by coalescence [2] and thermodynamic models [3]. In the coalescence picture, the density of the cluster is proportional to the proton density times the probability of finding a neutron within a small sphere of radius around the proton momentum. Nucleon coalescence mechanism can be described as:

$$E_A \frac{d^3 N_A}{d^3 p_A} = B_A \left(E_p \frac{d^3 N_p}{d^3 p_p} \right)^Z \left(E_n \frac{d^3 N_n}{d^3 p_n} \right)^{A-Z} \approx B_A \left(E_p \frac{d^3 N_p}{d^3 p_p} \right)^A, \quad (1)$$

where $E_p \frac{d^3 N_p}{d^3 p_p}$ is the Lorentz-invariant momentum distribution of proton, A is the mass number, Z is the proton number, $p_A = Ap_p$. The coalescence parameter, B_A , reflects the probability of nucleon coalescence, which is related to the local nucleon density [7].

Based on the coalescence picture, the yield ratio, $N(t) \cdot N(p) / N^2(d)$, is sensitive to the neutron density fluctuation, $\Delta n = \langle (\delta n)^2 \rangle / \langle n \rangle^2$, at kinetic freeze-out in relativistic heavy-ion collisions, where $\langle n \rangle$ denotes the average value over space and δn denotes the fluctuation of neutron density from its average value $\langle n \rangle$ [9]. In this case, the yield ratio of light nuclei can be approximated as:

$$N(t) \cdot N(p) / N^2(d) = g(1 + \Delta n), \text{ with } g = 0.29. \quad (2)$$

In heavy-ion collisions, the created matter is expected to develop strong baryon density fluctuation [4]. When its evolution trajectory in the QCD phase diagram passes across the first-order phase

25 transition line, a rapid increase of correlation length in the critical region has emerged as a results
 26 of the spinodal instability or approaches the CEP [9]. Therefore, light nuclei production at kinetic
 27 freeze-out in relativistic heavy-ion collisions may provide a unique probe to the critical endpoint in
 28 the QCD phase diagram.

29 2. Results and discussions

30 2.1 Transverse momentum spectra

31 The results are based on RHIC Beam Energy Scan I (BES-I) and are obtained for Au+Au col-
 32 lisions at $\sqrt{s_{NN}} = 7.7-200$ GeV at midrapidity. The main detectors used to obtain the results are the
 33 Time Projection Chamber (TPC) [5] and Time-Of-Flight (TOF) detectors [6]. The transverse momen-
 34 tum spectra of identified d (left panel), \bar{d} (middle panel), and t (right panel) are shown in Fig. 1. Due
 35 to limited statistics, there are not enough candidates to show the \bar{d} spectra at $\sqrt{s_{NN}} = 7.7$ GeV [7].
 36 The spectra are fitted with individual blast-wave functions and show a hardening with increasing
 multiplicity/centrality [11]. The blast-wave fits are shown as dashed lines in Fig. 1.

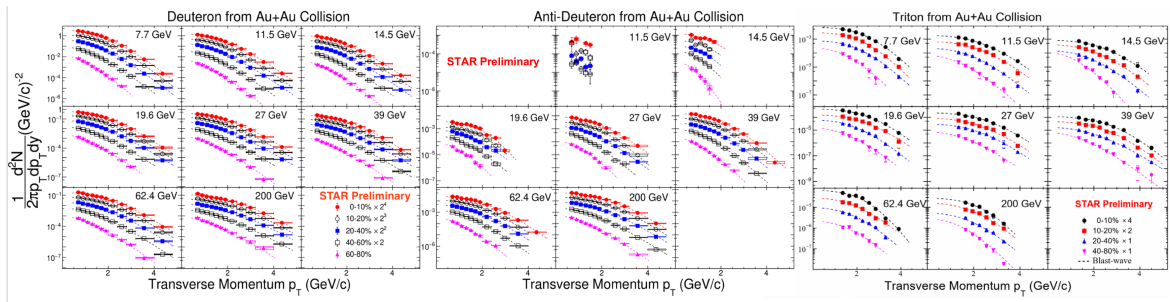


Fig. 1. Transverse momentum spectra of d (left), \bar{d} (middle), and t (right) measured at midrapidity in Au+Au collisions at $\sqrt{s_{NN}} = 7.7-200$ GeV for different collision centralities. The dashed lines are the individual fits to the data with blast-wave functions. Both the statistical and systematic error are shown.

37

38 2.2 Coalescence parameters

39 In the coalescence picture, the coalescence parameter, B_A , reflects the probability of nucleon co-
 40 alescence, which is related to the local nucleon density. The reference proton spectra for coalescence
 41 parameter extraction are from previous measurements by STAR [12]. In the left panel of Fig. 2, the
 42 p_T/A dependence of B_3 is shown at $\sqrt{s_{NN}} = 7.7$ and 200 GeV for different collision centralities. It
 43 is found that B_3 increases with increasing p_T/A , which might suggest an expanding collision sys-
 44 tem. The value of B_3 decreases from peripheral to central collisions, which can be explained by a
 45 decreasing source volume. In the right panel of Fig. 2, we compare the results of B_2 and $\sqrt{B_3}$ in the
 46 0-10% collision centrality at $p_T/A = 0.65$ GeV/c. It is found that B_2 and $\sqrt{B_3}$ are consistent within
 47 uncertainties except for $\sqrt{s_{NN}} = 200$ GeV. Below 20 GeV, the coalescence parameters B_2 and $\sqrt{B_3}$
 48 decrease with collision energy implied that particle-emitting source increase. When $\sqrt{s_{NN}} > 20$ GeV,
 49 the decreasing trend seems to change and saturate at BES energy, which might imply a dramatic
 50 change of the equation of states of the medium in the collision. At $\sqrt{s_{NN}} = 200$ GeV, B_2 and $\sqrt{B_3}$
 51 are different, which might due to the production mechanism for d and t are different.

52 2.3 Integral yields and particle ratios

53 The yields of triton and deuteron are obtained by measured p_T range and extrapolated to the
 54 unmeasured p_T regions with various parameterizations. The extrapolation is done by the individual

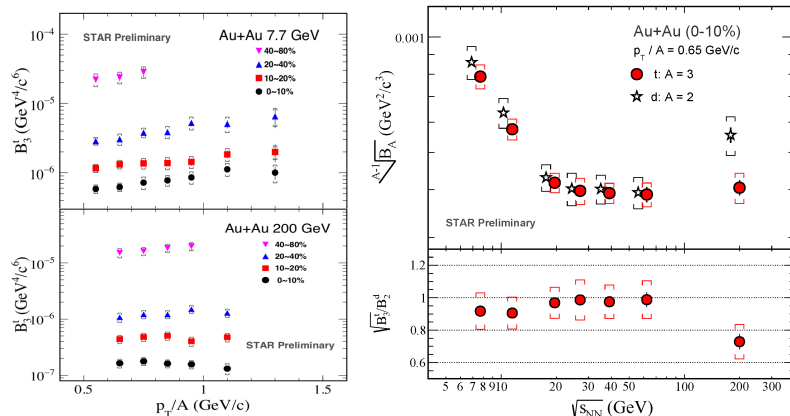


Fig. 2. (Left panel) Coalescence parameter B_3 as a function of p_T/A for triton from 7.7 and 200 GeV in 0-10%, 10-20%, 20-40% and 40-80% central Au+Au collisions. (Right panel) Coalescence parameter B_2 (open star) and $\sqrt{B_3}$ (red dot) as a function of collision energy in 0-10% central Au+Au collisions. The vertical lines and square brackets show the statistical and systematic errors, respectively.

55 blast-wave fits [11]. We also show the yield ratios of d/p , t/p , and t/d as a function of collisions
 56 energy in 0-10% central Au+Au collision in Fig. 3. The proton yields are corrected for the feed-down
 57 contribution [12]. The dashed lines are the thermal model calculations, which employ parameters
 58 established from the analysis of light hadron production in relativistic nuclear collisions. The thermal
 model describes the ratios of d/p very well but overestimate the t/p and t/d particle ratios [8, 13].

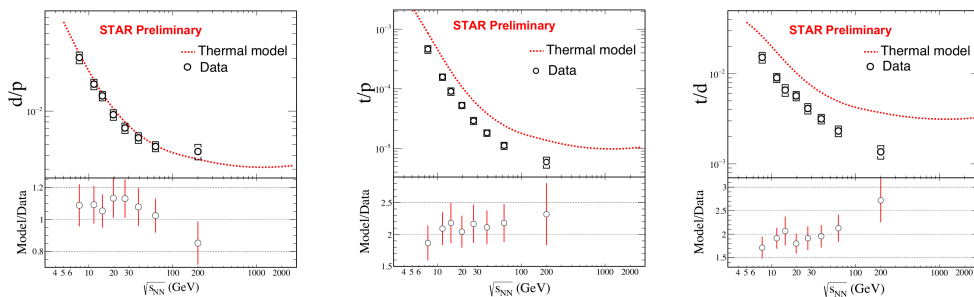


Fig. 3. d/p (left panel), t/p (middle panel), and t/d (right panel) ratios for 0-10% central Au+Au collisions at BES-I energies. The dotted lines are thermal model predictions. The errors combined the systematic and statistical uncertainties.

59

60 2.4 Neutron density fluctuation

61 The neutron density fluctuation, Δn , extracted from yield of light nuclei is presented in Fig. 4. A
 62 maximum around $\sqrt{s_{NN}} = 20$ GeV is found. This non-monotonic behavior indicates that the density
 63 fluctuations become the largest in collisions at this energy. When the evolution trajectory approaches
 64 the critical endpoint, the correlation length increases dramatically [10], and the density fluctuation
 65 enhances accordingly and reaches its maximum. The baryon density fluctuations are expected to be
 66 negligible if the phase transition from QGP to the hadronic matter is a crossover. Therefore, nucleon
 67 density fluctuations at kinetic freeze-out in relativistic heavy-ion collisions may provide a unique
 68 probe to the critical endpoint in the QCD phase diagram, which need further studies, especially the
 69 precise measurements and theoretical understanding.

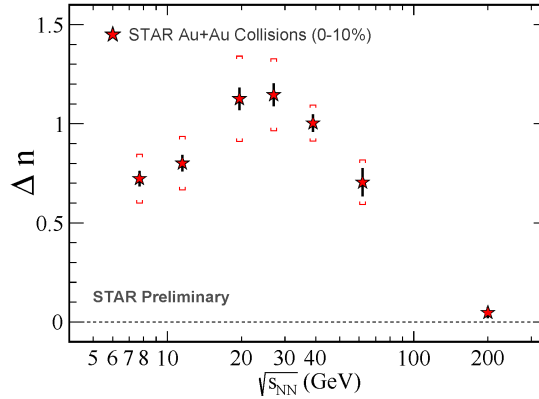


Fig. 4. The neutron density fluctuation, Δn , shows a non-monotonic behavior on collision energy and peaks at around 20 GeV. The vertical lines and square brackets show the statistical and systematic errors, respectively.

3. Conclusions

We present systematic studies of d and t production in heavy-ion collisions at $\sqrt{s_{NN}} = 7.7$ -200 GeV. The extracted coalescence parameter B_3 decreases with increasing collision energy and increases with increasing transverse momentum. The values of B_2 for deuteron and B_3 for triton decrease as collision energy increases and seem to reach a minimum around 20 GeV, indicating a change in the equation of state. The values of B_2 and $\sqrt{B_3}$ from central collision shows the same trends excepted at 200 GeV, which might imply a different formation mechanism for triton and deuteron at the top RHIC energy. The d/p ratio can be reproduced by the thermal model but it cannot describe the triton production. We also measured the collision-energy dependence of neutron density fluctuation and a non-monotonic energy dependence with a peak at around 20 GeV was found, which may indicate that the thermodynamic evolution trajectories of the system pass through the critical region.

Acknowledgement

This work is supported by the National Natural Science Foundation of China under Grants (No. 11890711, 11575069, 11828501 and 11861131009), Fundamental Research Funds for the Central Universities No. CCNU19QN054.

References

- [1] K. Fukushima and C. Sasaki, *Prog. Part. Nucl. Phys.* **72**, 99 (2013)
- [2] L. P. Csernai and J. I. Kapusta, *Phys. Rept.* **131**, 223 (1986).
- [3] A. Z. Mekjian, *Phys. Rev. C* **17**, 1051 (1978).
- [4] M. A. Stephanov, K. Rajagopal and E. V. Shuryak, *Phys. Rev. Lett.* **81**, 4816 (1998)
- [5] M. Anderson *et al.*, *Nucl. Instrum. Meth. A* **499**, 659 (2003)
- [6] W. J. Llope, *Nucl. Instrum. Meth. B* **241**, 306 (2005).
- [7] J. Adam *et al.* [STAR Collaboration], *Phys. Rev. C* **99**, no. 6, 064905 (2019)
- [8] N. Yu and X. Luo, *Eur. Phys. J. A* **55**, no. 2, 26 (2019)
- [9] K. J. Sun, L. W. Chen, C. M. Ko, J. Pu and Z. Xu, *Phys. Lett. B* **781**, 499 (2018)
- [10] B. Berdnikov and K. Rajagopal, *Phys. Rev. D* **61**, 105017 (2000)
- [11] E. Schnedermann, J. Sollfrank and U. W. Heinz, *Phys. Rev. C* **48**, 2462 (1993)
- [12] L. Adamczyk *et al.* [STAR Collaboration], *Phys. Rev. Lett.* **121**, no. 3, 032301 (2018)
- [13] A. Andronic, P. Braun-Munzinger, J. Stachel and H. Stocker, *Phys. Lett. B* **697**, 203 (2011)